ME 402 GRADUATE PROJECT REPORT

ACTIVE BATTERY COOLING SYSTEM FOR ALL-ELECTRIC VEHICLES

BY

JINGWEI ZHU

Department of Mechanical Science and Engineering
University of Illinois at Urbana-Champaign
Urbana, Illinois

Instructor:

Professor Stefan Elbel

Executive Summary

In this project, battery cooling systems using either liquid coolant or refrigerant for all-electric vehicles were investigated. Finite element analysis was carried out for the simulation of cooling performance of each battery cooling system design and was accomplished with Microsoft Excel. The initial and operating costs of each design were compared. A final design choice was provided based on the cooling performance, initial and operating costs. This design uses refrigerant directly for battery cell cooling, which is efficient in initial and space costs. It can keep the highest temperature of each battery cell in the range of 24.1~25.4℃. The additional operating costs to overcome the pressure drops in battery module cooling tubes are only 2W for each battery module.

Introduction

Power consumption, driving range and battery life are among the most important factors of electric vehicles. The performance and life of rechargeable lithium-ion batteries used to power electric vehicles can be significantly influenced by the battery temperature. At low temperatures, batteries have larger internal resistance and lower capacity due to poor ion transport (Figure 1). On the other hand, at elevated temperatures batteries have reduced cycle life due to loss of cyclable lithium and active material (Figure 2). The desired battery operating temperature is between 15℃ and 35℃ [1]. Battery thermal management system that keeps the battery temperature in the desired range can significantly improve electric vehicle power consumption and extend driving range as well as life of battery.

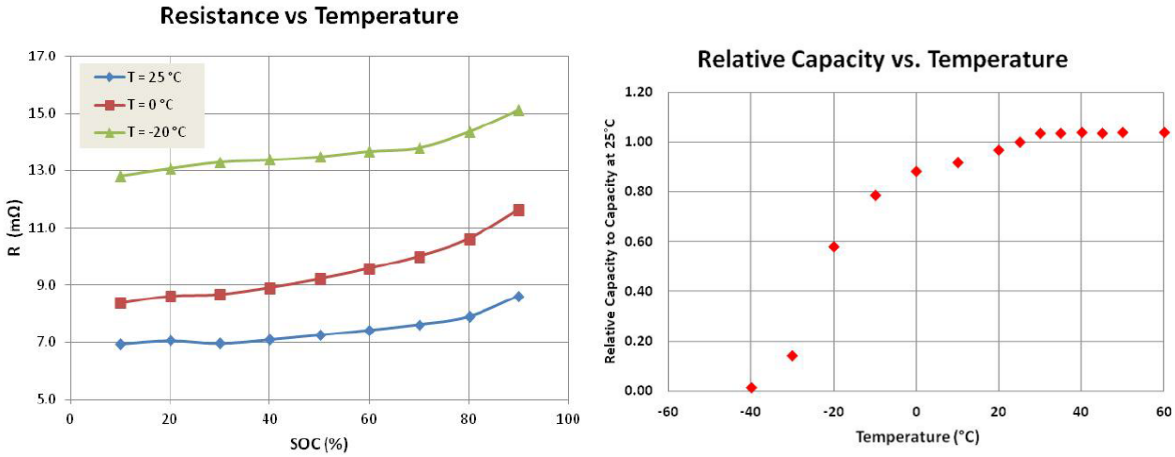

(a) (b)

Figure 1: Low temperature impact on (a) battery internal resistance and (b) battery capacity [1].

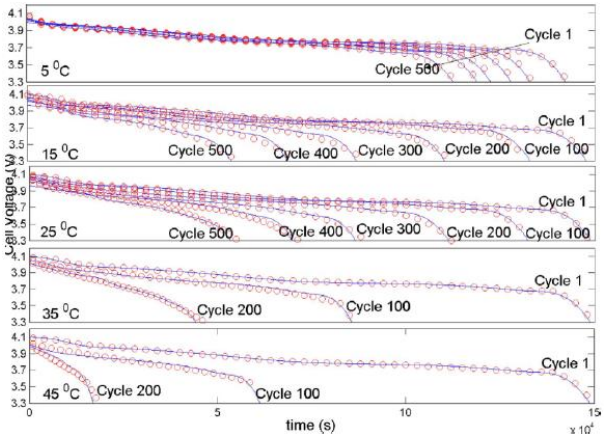

Figure 2: High temperature impact on battery cycle life [1].

Battery thermal management systems can provide either heating or cooling to the batteries according to the battery temperatures. For all-electric vehicles, battery heating can be achieved by using electric heaters or heat pumps. For hybrid vehicles, battery pack can also be heated by engine coolant so that engine waste heat is utilized. Battery cooling can be generally divided into two categories: passive cooling and active cooling. Passive systems directly use ambient air to cool the battery pack while in active cooling systems cabin air, liquid coolant, or refrigerant are circulated to transfer heat from the battery to the ambient. Table 1 summarizes the electric vehicle battery cooling systems used by some of the major electric vehicle manufacturers.

Table 1: Summary of electric vehicle battery cooling systems.

Make & Model	Active/Passive Cooling	Coolant	Battery
2016 Nissan LEAF SV (100% EV)	Passive (forced air convection)	Air	30kWh lithium-ion battery; 107 mile range
Nissan e-NV200 (concept commercial van; 100% EV)	Active (draw air from the vehicle's climate control system and channel the air over the battery cells)	Air	-
2016 GM Volt (hybrid)	Active	Liquid	18.4kWh compact power lithium-ion cells in the T-shaped battery pack; all-electric range 53 miles
Tesla Model S (100% EV)	Active	Glycol-based coolant (50% Sierra Glycol solution, 50% water)	70 kWh or 85 kWh microprocessor controlled, cylindrical lithium ion cells dubbed 18650s (248 ~ 287 mile range)

2016 Ford Focus Electric (all-electric)	Active	Liquid	23 kWh liquid-cooled, lithium-ion battery; 76 mile range
BMW i3 (all-electric)	Active	Direct refrigerant cooling (no extra installation in vehicle, use of existing A/C system)	22 kWh; 81 miles per charge;150 mile total range per charge with the BMW i3 with range extender (BMW is offering a gasoline range extender engine as an option)

In this project, active battery cooling systems using liquid coolant or refrigerant were studied.

Project Objectives

1. Design an active cooling system using liquid coolant or refrigerant for Tesla Model S battery pack in order to keep the battery temperature between 15°C and 35°C.
2. Compare the cooling performance of liquid coolant and refrigerant battery cooling systems at steady state by numerical simulation.
3. Compare the initial and operating costs of liquid coolant and refrigerant battery cooling systems.

Description of Approach

Tesla Model S battery pack

Tesla offers several variants of Model S with different battery capacities and electric ranges. The 85 kWh battery pack contains 7,104 lithium-ion Panasonic 18650 battery cells in 16 modules wired in series (14 in the flat section and two stacked on the front, as shown in Figure 3(a)) while the 60 kWh battery pack is composed of 14 modules with 6216 cells in total. Each battery module contains six groups of 74 cells wired in parallel; the six groups are then wired in series within the module. The cylindrical battery cells are packed in a beehive type configuration so that the space is most efficiently utilized (Figure 3(b)).

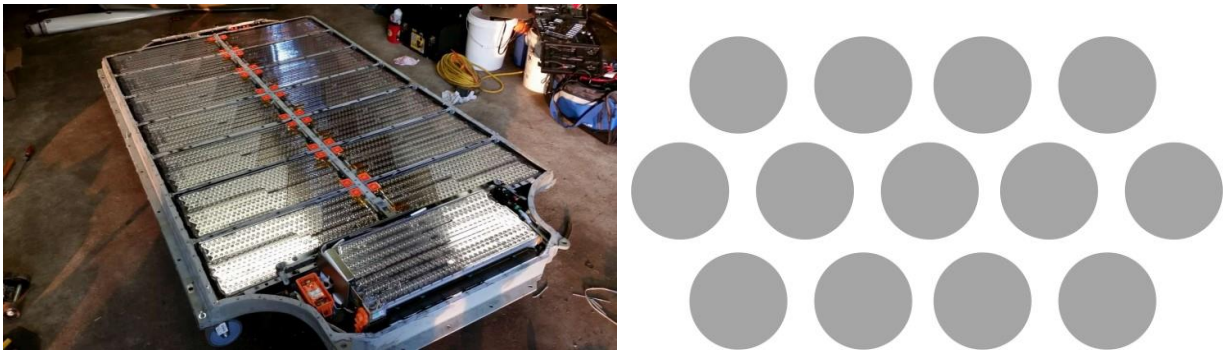

(a) (b)

Figure 3: (a) Tesla Model S battery pack and (b) cells in a beehive type configuration.

Since the Tesla Model S battery modules are identical, only the cooling of one module was studied and the results are applicable to the whole battery pack.

Layout of the active battery cooling system

In this project, a total of 441 battery cells in 14 rows (444 cells in a Tesla battery module) are assumed to be placed on and have good thermal contact with an aluminum plate. Cooling tubes are buried in the aluminum plate and also have good thermal contact with the plate. The arrangement of the cooling tubes with respect to the batteries in a battery module is shown in Figure 4. Two independent cooling tubes are stacked up which allow parallel or counter flowing cooling fluids (Figure 5).

Two types of active battery cooling systems, i.e. using liquid coolant or using refrigerant directly, were considered in this project. The schematics of active battery cooling systems using liquid coolant or refrigerant are shown in Figure 6. An additional liquid coolant loop with coolant pump is introduced in addition to the major A/C loop for active battery cooling system using liquid coolant. Heat is rejected from the liquid coolant loop to the major A/C loop through a plate heat exchanger, which is the evaporator in the A/C loop. For active battery cooling system using refrigerant, refrigerant in the A/C loop is fed to the battery pack directly. Additional liquid pump is not needed in this case, which saves both initial costs and space.

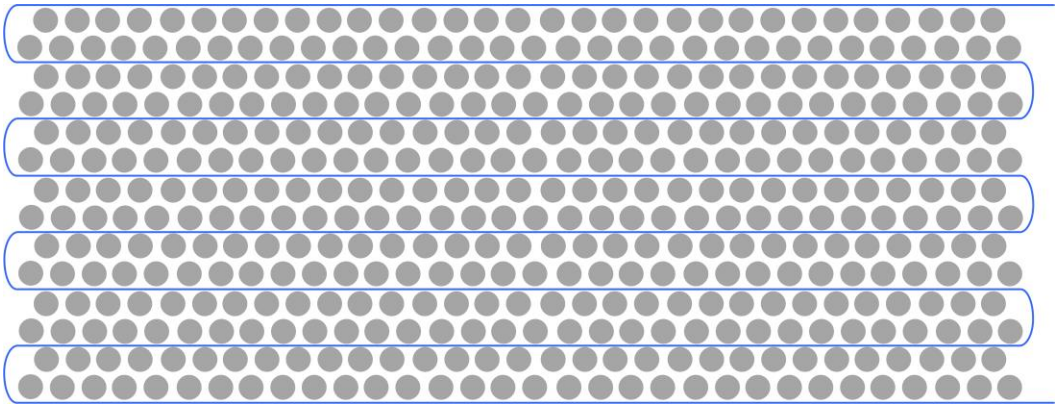

Figure 4: Cooling tube arrangement in a battery module.

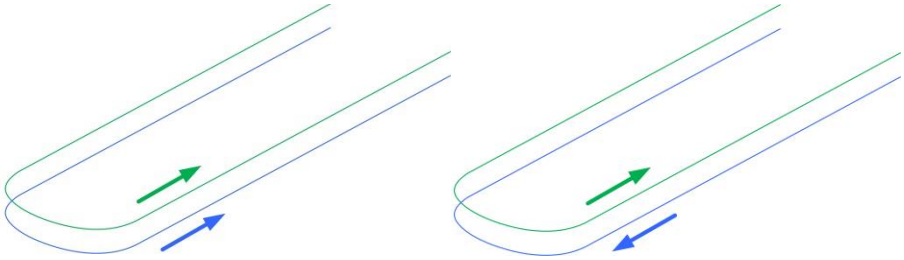

(a) (b)

Figure 5: (a) Parallel and (b) counter-flowing cooling fluids in the stacked cooling tubes.

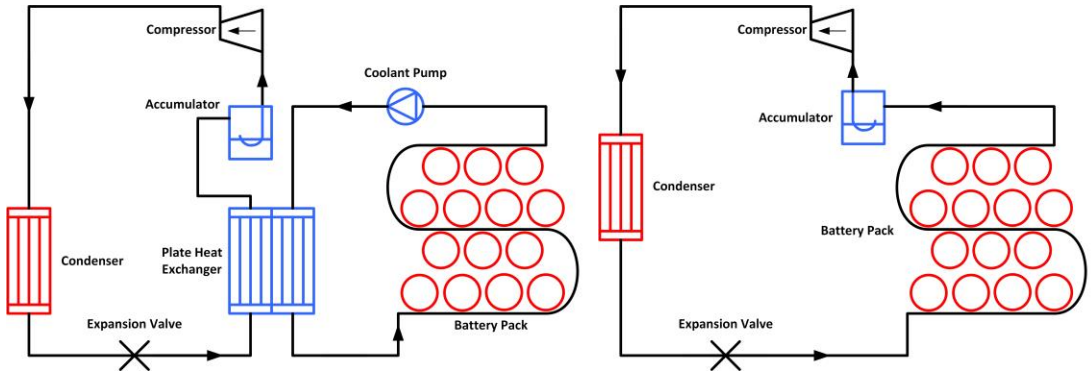

(a) (b)

Figure 6: Schematics of active battery cooling systems using (a) liquid coolant and (b) refrigerant directly.

Thermal modeling for the battery cells at steady state

Some important parameters of the 18650 battery cells are summarized in Table 2.

Table 2: 18650 battery cell parameters.

Diameter (mm)	Height (mm)	Thermal conductivity in the axial direction ($\frac{W}{m*K}$)	Voltage (V)	Max. discharge current (A)	Internal resistance (ohm)
18.3	64.8	28.05 [2]	3.6~3.7	4.3	~0.15 [3]

For simplicity of analysis, the battery cells are approximated as square pillars with height and side length of 65mm and 16mm, respectively.

The battery cell is modeled as a block with constant heat source density α ($\frac{W}{m^3}$) distributed throughout and constant thermal conductivity k. The temperature distribution is assumed to be one-dimensional. By solving the energy balance equation, the temperature distribution at steady state is found to be $T = T_{top} - \frac{\alpha}{2k}x^2$ where T_{top} is the temperature of the cell top. x is the distance to the top of the cell. The cell power $\dot{W}_{cell} = \alpha * V_{cell} = -k_{axial}\frac{dT}{dx}_{bottom} A_{bottom}$ where V_{cell} is the volume of the cell, $\frac{dT}{dx}_{bottom}$ and A_{bottom} are the temperature gradient and cross-sectional area at the cell bottom.

In the following analysis, $\dot{W}_{cell} = I_{max} R^2_{internal} = 2.77W$, $V_{cell} = 1.66E-5m^3$, $\alpha = \frac{\dot{W}_{cell}}{V_{cell}} = 166676\frac{W}{m^3}$, $A_{bottom} = 2.56E-4m^2$. The highest temperature in the cell is $T_{max} = T_{top} = T_{bottom} + \frac{\alpha}{2k}h^2_{cell}$, which is the temperature of the cell top. h_{cell} is the height of the cell.

Thermal modeling for the aluminum plate at steady state

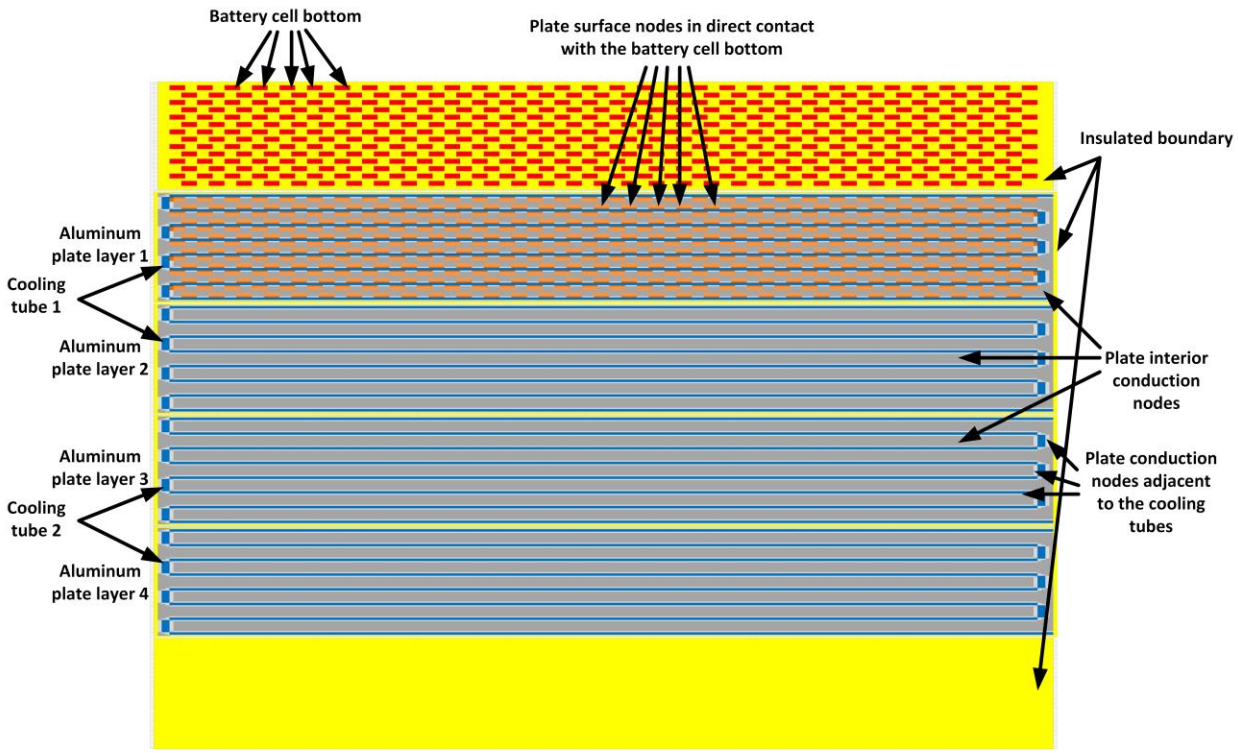

Figure 7: Finite element analysis domain for the aluminum plate.

Three-dimensional finite element analysis has been carried out in Microsoft Excel for the active battery cooling system. Increments in x, y, z direction are $\Delta x = \Delta y = \Delta z = 4\text{mm}$. The cooling tubes are simplified as square tubes and their side lengths are 8mm. The aluminum plate is separated into 4 layers. Cooling tube 1 occupies the first two layers while cooling tube 2 occupies layer 3 and 4. Two additional layers have been placed above and below the aluminum plate as insulated boundary, which is shown in yellow in Figure 7. The temperature of each node in the insulated boundary equals the temperature of the node next to it in the adjacent layer so that there is no heat transfer going through the insulated boundary. Battery cell bottom nodes (shown in red in Figure 7) are embedded in the top insulated boundary for computation of heat transfer between battery cells and aluminum plate. The aluminum plate is also assumed to be insulated at the four sides and this is modeled by adding insulated boundaries (shown in yellow in Figure 7) at the four sides as well. All the six layers have been shown in Figure 7.

The aluminum plate is divided into several domains. Steady state heat transfer equation for nodes in different domains is slightly different from each other.

i. Interior conduction node

3-D steady-state constant conductivity heat conduction with no heat generation:

$$\frac{\partial^2 T}{\partial x^2} + \frac{\partial^2 T}{\partial y^2} + \frac{\partial^2 T}{\partial z^2} = 0$$

$$\frac{\partial^2 T}{\partial x^2}_{i,j,k} \approx \frac{T_{i+1,j,k}+T_{i-1,j,k}-2T_{i,j,k}}{\Delta x^2}, \frac{\partial^2 T}{\partial y^2}_{i,j,k} \approx \frac{T_{i,j+1,k}+T_{i,j-1,k}-2T_{i,j,k}}{\Delta y^2}, \frac{\partial^2 T}{\partial z^2}_{i,j,k} \approx \frac{T_{i,j,k+1}+T_{i,j,k-1}-2T_{i,j,k}}{\Delta z^2}$$

Therefore

$$\frac{T_{i+1,j,k}+T_{i-1,j,k}-2T_{i,j,k}}{\Delta x^2}+\frac{T_{i,j+1,k}+T_{i,j-1,k}-2T_{i,j,k}}{\Delta y^2}+\frac{T_{i,j,k+1}+T_{i,j,k-1}-2T_{i,j,k}}{\Delta z^2}=0$$

$$T_{i,j,k}=(\frac{T_{i+1,j,k}+T_{i-1,j,k}}{\Delta x^2}+\frac{T_{i,j+1,k}+T_{i,j-1,k}}{\Delta y^2}+\frac{T_{i,j,k+1}+T_{i,j,k-1}}{\Delta z^2})/(\frac{2}{\Delta x^2}+\frac{2}{\Delta y^2}+\frac{2}{\Delta z^2})$$

ii. Conduction node next to cooling tubes

To simplify the analysis, the cooling tube wall is assumed to be of very large thermal conductivity and the tube wall temperature is uniform at each cross-section.

Assume the cooling fluid convective heat transfer coefficient at the inner tube surface is h_{cool} and the fluid temperature T_{cool} is uniform at each cooling tube cross-section. The conductivity of the conduction nodes is $k_A = 205 \frac{W}{m*K}$ (aluminum). The ratio between the outer perimeter and the inner perimeter of the tube is R. As an example, the steady state heat transfer equation for a node next to a cooling tube in the y direction is shown as follows:

$$\frac{2k_A h_{cool}/R}{\Delta y * h_{cool}/R + 2k_A} * (T_{cool} - T_{i,j,k}) * \Delta x \Delta z + k_A * \frac{T_{i-1,j,k} - T_{i,j,k}}{\Delta x} * \Delta y \Delta z + k_A * \frac{T_{i+1,j,k} - T_{i,j,k}}{\Delta x} * \Delta y \Delta z + k_A * \frac{T_{i,j,k+1} - T_{i,j,k}}{\Delta z} * \Delta x \Delta y + k_A * \frac{T_{i,j,k-1} - T_{i,j,k}}{\Delta z} * \Delta x \Delta y + k_A * \frac{T_{i,j-1,k} - T_{i,j,k}}{\Delta y} * \Delta x \Delta z = 0$$

$$T_{i,j,k} = \frac{\frac{2k_A h_{cool}/R}{\Delta y^2 * h_{cool}/R + 2k_A \Delta y} * T_{cool} + k_A * \frac{T_{i-1,j,k}}{\Delta x^2} + k_A * \frac{T_{i+1,j,k}}{\Delta x^2} + k_A * \frac{T_{i,j,k+1}}{\Delta z^2} + k_A * \frac{T_{i,j,k-1}}{\Delta z^2} + k_A * \frac{T_{i,j-1,k}}{\Delta y^2}}{\frac{2k_A h_{cool}/R}{\Delta y^2 * h_{cool}/R + 2k_A \Delta y} + \frac{2k_A}{\Delta x^2} + \frac{2k_A}{\Delta z^2} + \frac{k_A}{\Delta y^2}}$$

iii. Conduction only; at the bottom of each battery cell

Assume that the battery cell has perfect thermal contact with the aluminum plate. Consider the case in which the node is below the conductor-battery interface. Thermal conductivity of the conduction plate is k_A. The battery cell bottom node:

$$k_A * \frac{T_{bottom} - \bar{T}_{i,j,k}}{\frac{\Delta z}{2}} * A_{bottom} = \dot{W}_{cell}$$

$$T_{bottom} = \frac{\dot{W}_{cell} \Delta z}{2k_A A_{bottom}} + \bar{T}_{i,j,k}$$

$\bar{T}_{i,j,k}$ is the average temperature of conduction nodes below the battery cell.

For the node in the aluminum plate below the conductor-battery interface:

$$k_A * \frac{T_{bottom} - T_{i,j,k}}{\Delta z^2/2} + k_A * (\frac{T_{i+1,j,k} - T_{i,j,k}}{\Delta x^2} + \frac{T_{i-1,j,k} - T_{i,j,k}}{\Delta x^2} + \frac{T_{i,j-1,k} - T_{i,j,k}}{\Delta y^2} + \frac{T_{i,j+1,k} - T_{i,j,k}}{\Delta y^2} + \frac{T_{i,j,k-1} - T_{i,j,k}}{\Delta z^2}) = 0$$

$$T_{i,j,k} = \frac{\left[\frac{2T_{battery\ bottom}}{\Delta z^2} + \left(\frac{T_{i+1,j,k}}{\Delta x^2} + \frac{T_{i-1,j,k}}{\Delta x^2} + \frac{T_{i,j-1,k}}{\Delta y^2} + \frac{T_{i,j+1,k}}{\Delta y^2} + \frac{T_{i,j,k-1}}{\Delta z^2}\right)\right]}{\frac{3}{\Delta z^2} + \left(\frac{2}{\Delta x^2} + \frac{2}{\Delta y^2}\right)}$$

Thermal modeling for the cooling tubes at steady state

To simplify the modeling, it is assumed that there is no heat transfer between the two cooling tubes stacked together. Heat transfer only takes place between the cooling tubes and the aluminum plate.

Temperature increase and heat transfer through the cooling tube over a small distance Δl along the cooling fluids flowing direction can be approximated as:

$$\frac{2k_A h_{cool}/R}{\Delta y * h_{cool}/R + 2k_A} * (\bar{T}_{ambient} - \bar{T}_{cool}) * P_{surface} * \Delta l + \dot{m}_{cool} * C_{p_{cool}} * (T_k - T_{k+1}) = 0$$

where h_{cool} is the coolant heat transfer coefficient, $\bar{T}_{ambient}$ is the average temperature of the conduction nodes surrounding the coolant tube, $\bar{T}_{cool}$ is the average coolant temperature over the small distance, $P_{surface}$ is the outer contact perimeter of coolant tubes with the aluminum plate, $\dot{m}_{cool}$ is the mass flow rate of coolant flow, $C_{p_{cool}}$ is the specific heat capacity of the coolant, T_k is the temperature of coolant inflow and T_{k+1} is the temperature of coolant outflow. $\bar{T}_{cool}$ is approximated as $\frac{T_{k+1}+T_k}{2}$. Heat conduction in the flow direction is neglected.

$$T_{k+1} = (\frac{2k_A h_{cool}/R}{\Delta y * h_{cool}/R + 2k_A} * (\bar{T}_{ambient} - \frac{T_k}{2}) * P_{surface} * \Delta l + \dot{m}_{cool} * C_{p_{cool}} * T_k)/(\dot{m}_{cool} * C_{p_{cool}} + \frac{k_A h_{cool}/R}{\Delta y * h_{cool}/R + 2k_A} * P_{surface} * \Delta l)$$

i. Liquid coolant

Nusselt number for single-phase laminar flow (Re<2300) in square tubes is approximately 3.3.

$$\overline{Nu} = \frac{h_{cool} D_h}{k_{cool}} = 3.3$$

Therefore, for laminar flow, heat transfer coefficient h_{cool} is $3.3k_{cool}/D_h$.

Heat transfer coefficient for single-phase turbulent flow ($2300 \leq Re_D \leq 120000$) can be achieved by applying Dittus-Boelter equation:

$$h_{cool} = 0.023\left(\frac{k_{cool}}{D_h}\right)Re_D^{0.8}Pr^{0.4}$$

In the following design analysis, the liquid coolant used is 50-50% water-glycol mixture. Properties of the coolant are summarized in Table 3 [4]:

Table 3: Summary of the liquid coolant properties [4].

Heat capacity $(\frac{J}{kg*K})$	Density (kg/m^3)	Thermal conductivity $(\frac{W}{m*K})$	Kinematic viscosity (m^2/s)	Coolant Prandtl number (-)
3200	1092	0.405	9E-6	7.77E1

ii. Refrigerant (two-phase)

Chen's correlation for boiling heat transfer to saturated fluids in convective flow [5] is used to calculate the heat transfer coefficient of the refrigerant flow.

$$h_{cool} = h_{micro} + h_{macro}$$

$$h_{macro} = 0.023(Re_l)^{0.8}(Pr_l)^{0.4}\left(\frac{k_l}{D}\right)F$$

F is defined as $\left(\frac{\mathrm{Re}}{\mathrm{Re_l}}\right)^{0.8}$, $\mathrm{Re} = \mathrm{Re_l F}^{1.25}$ is the effective Reynolds number for the two-phase flow.

$$h_{micro} = 0.00122\left(\frac{k_l^{0.79}C_{pl}^{0.45}\rho_l^{0.49}g_c^{0.25}}{\sigma^{0.5}\mu_l^{0.29}\lambda^{0.24}\rho_v^{0.24}}\right)(\Delta T)^{0.24}(\Delta P)^{0.75}S$$

S is defined as the ratio of the effective superheat to the total superheat of the wall: $\mathrm{S} = \left(\frac{\Delta \mathrm{T_e}}{\Delta \mathrm{T}}\right)^{0.99}$

σ is the vapor-liquid surface tension, λ is the latent heat of vaporization, $\Delta \mathrm{T} = \mathrm{T_w} - \mathrm{T_{sat}}$, ΔP is the difference in vapor pressure corresponding to ΔT ($\frac{\Delta \mathrm{P}}{\Delta \mathrm{T}} = \frac{\lambda \rho_\mathrm{v}}{\mathrm{T}}$, Clausius and Clapeyron equation).

$$F \approx 3 * \left(\frac{1}{x_{tt}}\right)^{0.684} (x_{tt} < 5)$$

$$F = 1\ (x_{tt} \geq 5)$$

$\mathrm{x_{tt}}$ is Martinelli parameter $\left(\frac{1-\mathrm{x}}{\mathrm{x}}\right)^{0.9}\left(\frac{\rho_\mathrm{v}}{\rho_\mathrm{l}}\right)^{0.5}\left(\frac{\mu_\mathrm{l}}{\mu_\mathrm{v}}\right)^{0.1}$

$$S \approx -0.5\, log_{10}\, Re + 2.9\ \ (Re < 4E5)$$

$$S = 0.1\ (Re \geq 4E5)$$

The refrigerant used in the following analysis is R134a. Its properties at specific saturation temperature are obtained by commercial software Engineering Equation Solver (EES). Saturated properties of R134a at 10℃ are shown in Table 4:

Table 4: Saturated properties of R134a at 10℃.

Saturated liquid Prandtl number (-)	Saturated liquid thermal conductivity ($\frac{W}{m*K}$)	Saturated liquidheat capacity ($\frac{J}{kg*K}$)	Saturated liquid density (kg/m^3)	Saturated vapor density (kg/m^3)	Vapor liquid surface tension (N/m)	Saturated liquid dynamic viscosity ($\frac{kg}{m*s}$)	Saturated vapor dynamic viscosity ($\frac{kg}{m*s}$)	Latent heat of vaporization (J/kg)
3.555	0.09023	1.37E3	1.26E3	2.02E1	1E-2	2.34E-4	1.132E-5	1.91E5

Pressure drop in the cooling tubes

i. Liquid coolant

Darcy friction factor $f = \frac{\Delta P}{L}\frac{2D_h}{\rho v^2}$

For laminar flow in square channel: $f = \frac{56.9}{Re_D}$

For turbulent flow: $f = 0.25\left[\log_{10}(\frac{\epsilon}{3.7D} + \frac{5.74}{Re^{0.9}})\right]^{-2}$ (Swamee-Jain equation)

Very smooth tube surface is assumed: $\epsilon = 0.0015\text{mm}$.

ii. Refrigerant (two-phase)

Choi's pressure drop correlation for evaporation of refrigerants in smooth tubes [6] is used to calculate the pressure drop of the refrigerant flow in the cooling tubes.

$$\Delta P_{tp} = \Delta P_{friction} + \Delta P_{acceleration} = \left(\frac{f_N L(\nu_{out} + \nu_{in})}{D_h} + (\nu_{out} - \nu_{in})\right)G^2$$

$f_N = 0.00506 Re_l^{-0.0951} K_f^{0.1554}$, $Re_l = \frac{GD_h}{\mu_l}$, $K_f = \frac{\Delta x h_{fg}}{Lg}$

ν_{in} and ν_{out} are specific volumes at the inlet and outlet, L is the tube length, G is the mass flux, Re_l is the liquid Reynolds number.

Simulation Results

Finite element analysis results have been shown for each following configuration. The distribution of the highest temperature in every battery cell (i.e. T_{top}) for each case has been shown. Each red block is a battery cell. They are packed closely without any gap between each other in the temperature distribution diagram. The real alignment of battery cells in the simulation has been shown in Figure 7 (top layer). There are 32 battery cells in each odd row and 31 in each even row.

For each case, $\dot{m}_{cool}$ is the mass flow rate in each cooling tube (Note: when the two cooling tubes are not connected with each other, the total mass flow rate of cooling fluids should be $2\dot{m}_{cool}$), R is the ratio of the cooling tube outer perimeter to the inner perimeter, D_h is the hydraulic diameter of the cooling tubes. Total length of each cooling tube is $L = 7.384m$.

For liquid coolant, the coolant temperature at the cooling tube inlets is set to $T_{cool,in} = 10°C$; for refrigerant, the saturated temperature is set to be 10°C as well and the two-phase flow quality at the cooling tube inlets is set to x_{in}=0.22, which is the quality of saturated R134a at 10°C after isenthalpic expansion from saturated liquid at 40°C.

Liquid coolant, laminar, counter-flow

i. $\dot{m}_{cool} = 0.05kg/s$, $T_{cool,in} = 10°C$, $R = 2$, $D_h = 4mm$ (Re=1270), coolant enters through the upper-right and the lower-right corners

Figure 8: Distribution of highest temperature in each battery cell with counter-flowing coolant; $\dot{m}_{cool} = 0.05kg/s$, $T_{cool,in} = 10°C$, $R = 2$.

Heat transfer coefficient $h_{cool} = 334 \frac{W}{m^2K}$; heat removed by liquid coolant: 1224W; heat generation by battery cells:1223W; power discrepancy 0.08%; coolant outflow temperature: 13.83 and 13.81 °C; average flow velocity is 0.72m/s; pressure drop in each cooling tube: ΔP =23.084kPa. Battery cell temperatures are much higher than the desirable battery operating temperature range 15°C~35°C.

Liquid coolant, turbulent, counter-flow

i. $\dot{m}_{cool} = 0.04kg/s$, $T_{cool,in} = 10°C$, $R = 5$, $D_h = 1.6mm$ (Re=2540), coolant enters through the upper-right and the lower-right corners

Figure 9: Distribution of highest temperature in each battery cell with counter-flowing coolant; $\dot{m}_{cool} = 0.04kg/s$, $T_{cool,in} = 10°C$, $R = 5$.

Heat transfer coefficient $h_{cool} = 1.76E4 \frac{W}{m^2K}$; heat removed by liquid coolant: 1238W; heat generation by battery cells: 1223W; power discrepancy 1.23%; coolant outflow temperature: 14.84 and 14.72℃; average flow velocity is 14.31m/s; pressure drop in each cooling tube: ΔP =25716kPa.

ii. $\dot{m}_{cool} = 0.05kg/s$, $T_{cool,in} = 10℃$, $R = 5$, $D_h = 1.6mm$ (Re=3180), coolant enters through the upper-right and the lower-right corners

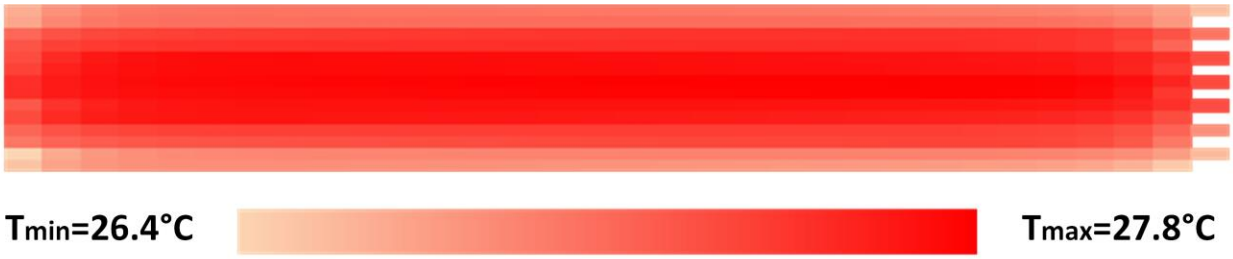

Figure 10: Distribution of highest temperature in each battery cell with counter-flowing coolant; $\dot{m}_{cool} = 0.05kg/s$, $T_{cool,in} = 10℃$, $R = 5$.

Heat transfer coefficient $h_{cool} = 2.1E4 \frac{W}{m^2K}$; heat removed by liquid coolant: 1242W; heat generation by battery cells:1223W; power discrepancy 1.55%; coolant outflow temperature: 13.88 and 13.76 ℃; average flow velocity is 17.89m/s; pressure drop in each cooling tube: ΔP =35973kPa.

iii. $\dot{m}_{cool} = 0.2kg/s$, $T_{cool,in} = 10℃$, $R \approx 1$, $D_h = 8mm$ (Re=2540), coolant enters through the upper-right and the lower-right corners

Figure 11: Distribution of highest temperature in each battery cell with counter-flowing coolant; $\dot{m}_{cool} = 0.2kg/s$, $T_{cool,in} = 10℃$, $R \approx 1$.

Heat transfer coefficient $h_{cool} = 3.52E3 \frac{W}{m^2K}$; heat removed by liquid coolant: 1253W; heat generation by battery cells: 1223W; power discrepancy 2.45%; coolant outflow temperature: 10.98 and 10.93℃; average flow velocity is 2.86m/s; pressure drop in each cooling tube: ΔP =195kPa.

Liquid coolant, turbulent, parallel-flow

i. $\dot{m}_{cool} = 0.04kg/s$, $T_{cool,in} = 10℃$, $R = 5$, $D_h = 1.6mm$ (Re=2540), coolant enters through the upper-right corner

Figure 12: Distribution of highest temperature in each battery cell with parallel-flowing coolant; $\dot{m}_{cool} = 0.04kg/s$, $T_{cool,in} = 10℃$, $R = 5$.

Heat transfer coefficient $h_{cool} = 1.76E4\frac{W}{m^2K}$; heat removed by liquid coolant: 1224W; heat generation by battery cells: 1223W; power discrepancy 0.08%; coolant outflow temperature: 14.83 and 14.74℃; average flow velocity is 14.31m/s; pressure drop in each cooling tube: ΔP =25716kPa.

Refrigerant, counter-flow

i. $\dot{m}_{cool} = 0.006kg/s$, $Re_l = 1.6E4$, $T_{sat} = 10℃$, $x_{in} = 0.22$, $R = 5$, $D_h = 1.6mm$, refrigerant enters through the upper-right and lower-right corners

Figure 13: Distribution of highest temperature in each battery cell with counter-flowing refrigerant; $\dot{m}_{cool} = 0.006kg/s$, $T_{sat} = 10℃$, $x_{in} = 0.22$, $R = 5$.

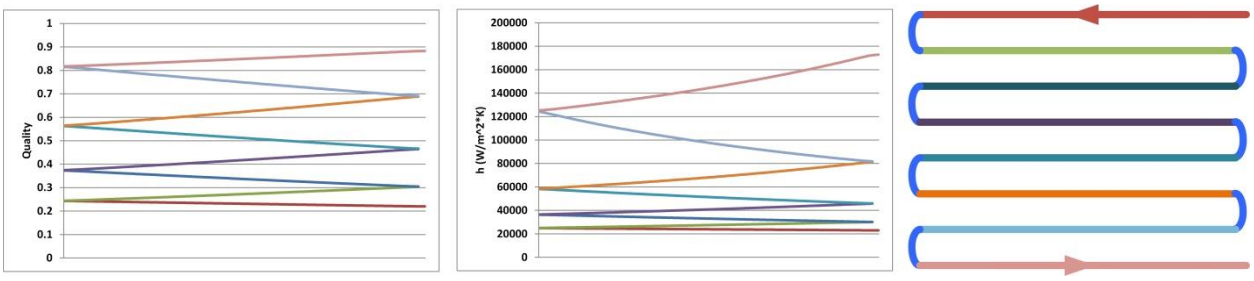

Figure 14: Variation of quality and heat transfer coefficient of the two-phase flow at different locations in the upper refrigerant loop; $\dot{m}_{cool} = 0.006kg/s$, $T_{sat} = 10℃$, $x_{in} = 0.22$, $R = 5$.

Heat removed by liquid coolant: 1320W; heat generation by battery cells: 1223W; power discrepancy 7.93%; refrigerant outflow quality: 0.883 and 0.708; ΔP = 9173kPa.

In Chen's correlation, it is assumed that the two-phase flow regime is always annular flow and liquid will attach to the wall. Therefore the correlated heat transfer coefficient seems to keep increasing with vapor quality. In reality this is not true. At high quality there will be dry-out of refrigerant taking place which

reduces the heat transfer efficiency. Heat transfer coefficient generally increases rapidly at low vapor quality, flattens out and eventually drops at high vapor quality.

ii. $\dot{m}_{cool} = 0.006 kg/s$, $Re_l = 3.2E3$, $T_{sat} = 10°C$, $x_{in} = 0.22$, $R \approx 1$, $D_h = 8mm$, refrigerant enters through the upper-right and lower-right corners

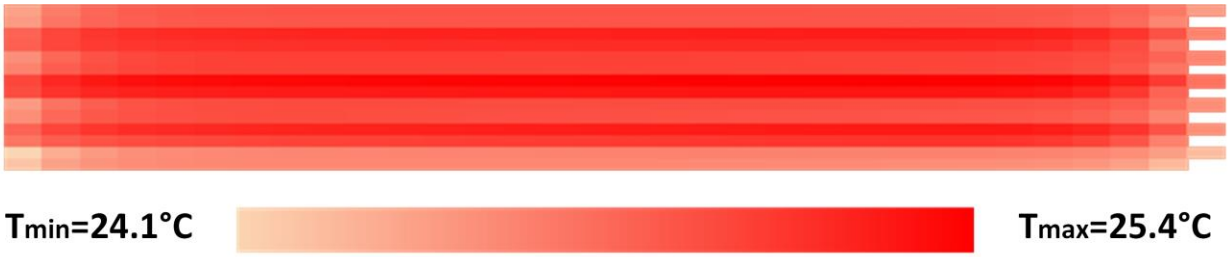

Figure 15: Distribution of highest temperature in each battery cell with counter-flowing refrigerant; $\dot{m}_{cool} = 0.006 kg/s$, $T_{sat} = 10°C$, $x_{in} = 0.22$, $R \approx 1$.

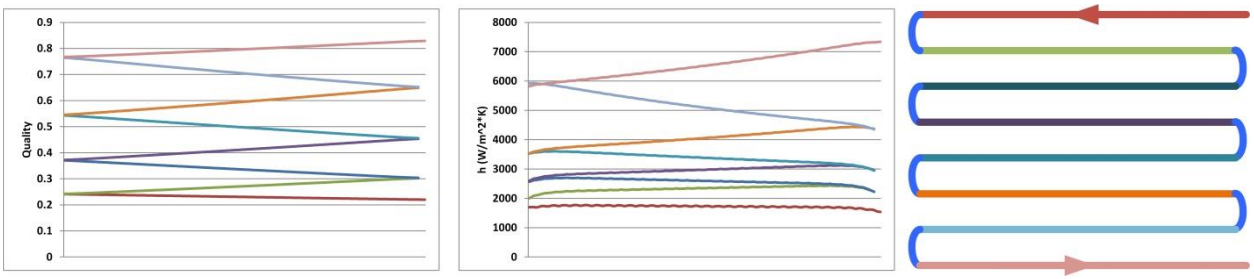

Figure 16: Variation of quality and heat transfer coefficient of the two-phase flow at different locations in the upper refrigerant loop; $\dot{m}_{cool} = 0.006 kg/s$, $T_{sat} = 10°C$, $x_{in} = 0.22$, $R \approx 1$.

Heat removed by liquid coolant: 1300W; heat generation by battery cells: 1223W; power discrepancy 6.30%; refrigerant outflow quality: 0.829 and 0.748; $\Delta P = 3.414 kPa$.

Refrigerant, parallel-flow

i. $\dot{m}_{cool} = 0.006 kg/s$, $Re_l = 1.6E4$, $T_{sat} = 10°C$, $x_{in} = 0.22$, $R = 5$, $D_h = 1.6mm$, refrigerant enters through the upper-right corner

Figure 17: Distribution of highest temperature in each battery cell with parallel-flowing refrigerant; $\dot{m}_{cool} = 0.006 kg/s$, $T_{sat} = 10°C$, $x_{in} = 0.22$, $R = 5$.

Heat removed by liquid coolant: 1320 W; heat generation by battery cells: 1223W; power discrepancy 7.93%; refrigerant outflow quality: 0.884 and 0.709; $\Delta P = 9183 kPa$.

ii. $\dot{m}_{cool} = 0.006kg/s$, $Re_l = 3.2E3$, $T_{sat} = 10℃$, $x_{in} = 0.22$, $R \approx 1$, $D_h = 8mm$, refrigerant enters through the upper-right corner

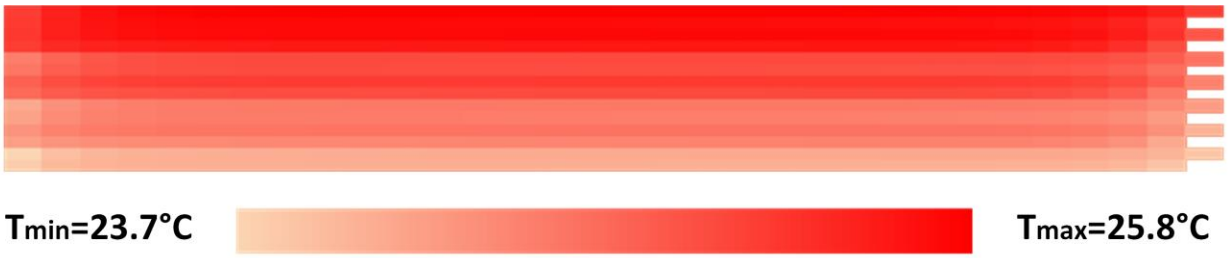

Figure 18: Distribution of highest temperature in each battery cell with parallel-flowing refrigerant; $\dot{m}_{cool} = 0.006kg/s$, $T_{sat} = 10℃$, $x_{in} = 0.22$, $R \approx 1$.

Heat removed by liquid coolant: 1300W; heat generation by battery cells: 1223W; power discrepancy 6.30%; refrigerant outflow quality: 0.829, 0.749; $\Delta P = 3.414kPa$.

Refrigerant, counter-flow, connecting the outlet of one cooling tube with the inlet of another tube

i. $\dot{m}_{cool} = 0.0095kg/s$, $Re_l = 5.07E3$, $T_{sat} = 10℃$, $x_{in} = 0.22$, $R \approx 1$, $D_h = 8mm$, refrigerant enters through the upper-right corner and exit through the upper-right corner

Figure 19: Distribution of highest temperature in each battery cell with counter-flowing refrigerant; the outlet of one cooling tube is connected with the inlet of another tube; $\dot{m}_{cool} = 0.\frac{0095kg}{s}$, $T_{sat} = 10℃$, $x_{in} = 0.22$, $R \approx 1$.

Heat removed by liquid coolant: 1270W; heat generation by battery cells: 1223W; power discrepancy 3.84%; refrigerant outflow quality: 0.923; $\Delta P = 9.163kPa$.

Discussion and Conclusions

Cooling performance observations

1. Cooling tubes in counter-flow configuration generally have more uniform temperature distribution compared with cooling tubes in parallel-flow configuration. Cooling efficiency is sacrificed for temperature uniformity. However, in the battery cooling applications, temperature uniformity is more important.
2. Cooling tubes inner diameter and cooling fluid mass flow rate need to be carefully chosen so that the cooling fluid Reynolds number is in the turbulent range. Turbulent flow has much higher heat transfer coefficient than laminar flow due to the better flow mixing and steeper temperature gradient.

3. Two-phase refrigerant flow has very different heat transfer coefficients at different qualities. However, the temperature distributions achieved with refrigerant cooling seems to be even more uniform than those with liquid coolant. This is mainly due to the constant refrigerant temperature in the cooling tubes as long as it is in two-phase. Moreover, the temperature differences between the refrigerant and the battery cells are small due to the high heat transfer coefficient of two-phase flow. Even though temperature difference at one location may be several times larger than another location when using refrigerant, satisfactorily uniform temperature distribution can still be achieved because of the small magnitude of temperature differences. For liquid coolant, heat transfer coefficient remains constant throughout the cooling tubes. However, coolant temperature may rise significantly along the flow direction as a result of heat absorption, which is the major contributor of non-uniform temperature distribution.
4. For refrigerant loop in parallel-flow configuration, battery cells which are closer to the refrigerant inlets have higher temperature. This is due to the lower heat transfer coefficient of refrigerant at lower vapor quality. On the contrary, for liquid coolant loop where the heat transfer coefficient remains constant throughout the loop, the closer to the coolant inlets, the lower the coolant temperature is and thus the battery cell temperature is lower.

Cost comparison

Initial and space costs of liquid coolant active battery cooling systems are higher than refrigerant systems because of the additional pump and larger size of evaporator needed for heat transfer between the coolant loop and the major A/C loop. The condenser, expansion valve, compressor and accumulator used in the A/C loop for each battery cooling system design are all the same. The costs of cooling tubes are assumed to be the same for different battery cooling system designs.

The operating costs of each battery cooling system are calculated for each configuration mentioned above. The total battery cooling system operating costs $C_{total} = C_{capacity} + C_{pressure\ drop}$ where $C_{capacity}$ is the costs required to generate the battery module cooling capacity in A/C loop (zero pressure drop in the evaporator and cooling tubes) and $C_{pressure\ drop}$ accounts for the costs associated with overcoming the pressure drop in the cooling tubes. For simplicity, the temperature difference between fluids and the pressure drop in the evaporator in liquid coolant systems is considered to be small and is not taken into account. Since the cooling capacity for the battery module is the same for each design (i.e. battery heat generation rate) and the liquid coolant inlet temperature equals the refrigerant saturated temperature in each design, $C_{capacity}$ is the same for each design. Only $C_{pressure\ drop}$ needs to be compared, which is the additional pump/compressor power needed to overcome the pressure drop in the cooling tubes for liquid coolant/refrigerant battery cooling systems. The pump power is assumed to be the power required to raise the pressure of liquid coolant by ΔP through an isentropic process. The compressor power is the power needed to raise the pressure of saturated vapor by ΔP through an isentropic process.

Table 5: Summary of additional pump/compressor operating costs $C_{pressure\ drop}$ for different battery cooling system designs.

Type	Liquid coolant					Refrigerant				
Laminar/turbulent	Laminar	Turbulent				Turbulent				
Counter/parallel-flow	Counter	Counter			Parallel	Counter		Parallel		Counter (connect one tube outlet with another tube inlet)
Case	i	i	ii	iii	i	i	ii	i	ii	i
ΔP (kPa)	23.1	25716	35973	195	25716	9173	3.4	9183	3.4	9.2
$\dot{m}_{cool,total}$ **(kg/s)**	0.1	0.08	0.1	0.4	0.08	0.012	0.012	0.012	0.012	0.0095
Additional operating costs (W)	2.311	2046	3569	78.02	2046	- (too large ΔP)	2.008	- (too large ΔP)	2.008	4.273

A summary of the additional pump/compressor operating costs $C_{pressure\ drop}$ for each battery cooling system design is provided in Table 5.

Final Design Choice

Counter-flowing refrigerant battery cooling system with $\dot{m}_{cool} = 0.006 kg/s$, $T_{sat} = 10°C$, $x_{in} = 0.22$, $R \approx 1$ (very thin cooling tube wall), $D_h = 8mm$ seems to be the best choice among all the configurations mentioned above considering the cooling performance (highest temperature of each battery cell in the range of 24.1~25.4°C), the initial and space costs (no additional pump needed) and the additional operating costs (2W for each battery module).

References

1. Pesaran, A. (2013). Addressing the Impact of Temperature Extremes on Large Format Li-Ion Batteries for Vehicle Applications.
2. Maleki, H., Al Hallaj, S., Selman, J. R., Dinwiddie, R. B., & Wang, H. (1999). Thermal Properties of Lithium - Ion Battery and Components. Journal of The Electrochemical Society, 146(3), 947-954.
3. http://lygte-info.dk/review/batteries2012/Common18650Summary%20UK.html
4. Bohne, D., Fischer, S., & Obermeier, E. (1984). Thermal, Conductivity, Density, Viscosity, and Prandtl - Numbers of Ethylene Glycol - Water Mixtures. Berichte der Bunsengesellschaft für physikalische Chemie, 88(8), 739-742.
5. Chen, J. C. (1966). Correlation for boiling heat transfer to saturated fluids in convective flow. Industrial & Engineering Chemistry Process Design and Development, 5(3), 322-329.
6. Choi, J. Y., Kedzierski, M. A., & Domanski, P. (1999). A generalized pressure drop correlation for evaporation and condensation of alternative refrigerants in smooth and micro-fin tubes. US Department of Commerce, Technology Administration, National Institute of Standards and Technology, Building and Fire Research Laboratory.